Effects of the Dzyaloshinskii-Moriya interaction on the Fermi-Pasta-Ulam behavior in a magnetic system

Jeramy Lewis [1,*] and Robert E. Camley [1,2]

[1] *Center for Magnetism and Magnetic Nanostructures, University of Colorado–Colorado Springs, Colorado Springs, Colorado 80918, USA*

[2] *UCCS BioFrontiers Center, University of Colorado–Colorado Springs, Colorado Springs, Colorado 80918, USA*

(Received 14 March 2023; accepted 9 June 2023; published 22 June 2023)

We study the behavior of nonlinear spin motion in one-dimensional magnetic chain models. We explore how the various parameters affect the phase transitions between linear and nonlinear behaviors both with and without the Dzyaloshinskii-Moriya interaction (DMI). A Fourier analysis method is employed to investigate the modes in the structure with DMI. In all cases, we find that uniaxial anisotropy is necessary for the Fermi-Pasta-Ulam effect to appear. We investigate the DMI influence through the use of phase diagrams that examine the transitions between the three fundamental states: linear, Fermi-Pasta-Ulam, and ergodic. The DMI does make significant changes in these phase diagrams because it allows for additional routes for the distribution of energy.

DOI: 10.1103/PhysRevB.107.224421

I. INTRODUCTION

Fermi, Pasta, and Ulam (FPU) addressed a fundamental issue in nonlinear physics through a numerical study of the vibrational motion of a one-dimensional linear chain [1]. Their expectation for a linear system was, if energy is put into one eigenmode, it will eventually be spread out equally through all the eigenmodes. This is the ergodic state. What they found, in contrast, for a nonlinear system was very different. Energy added to one mode was transferred to nearby modes in frequency, but then would nearly completely return to the original mode as time progressed. Ultimately, the energy remained in a small number of modes, cycling between these modes with a time that typically is several thousand periods of the original motion.

The FPU recurrence was explained by Zabusky and Kruskal through soliton dynamics [2]. They showed that, in the continuum limit, the FPU problem was related to the Korteweg de Vries differential equation and that a large amplitude periodic wave would decompose into solitons with different speeds. The collisions of the fast and slow solitons lead to a periodic reconstruction of the initial state.

Surprisingly, there has been relatively little work on the equivalent FPU problem in magnetic systems [3]. We recently showed [4] that it was possible to find FPU-like behavior in a chain of exchange-coupled spins, but only when some uniaxial anisotropy (or effective demagnetizing field) was present. A similar anisotropy requirement has been noted in other publications devoted to Dzyaloshinskii-Moriya interaction (DMI) [5]; this includes work on ferromagnetic waveguides [6], and quantum-state transfer and storage devices [7,8].

There are fundamental questions that still need to be answered. It is important to better understand the role of the uniaxial anisotropy, which is required to find the FPU behavior. Furthermore, magnetic systems with DMI provide interesting and fundamental twists to the problem in that the DMI creates a nonreciprocal spin-wave behavior [9–11]. A second important issue with DMI involves the identification of the linear eigenstates. The standing spin waves in a one-dimensional finite chain in a normal ferromagnet are no longer eigenmodes in a finite system with DMI. In contrast, the eigenmodes in a system with DMI have a drift velocity. The net result for the DMI case is that the nodes remain fixed in time while the antinodes drift with a constant velocity [9].

Exploring these issues may be of importance for both fundamental and experimental research efforts [10]. For example, Moon *et al.* performed a study of spin-wave properties in the presence of DMI in ferromagnetic/normal metal bilayers to investigate asymmetric spin-wave attenuation and excitation amplitudes [11]. Their results may be useful for characterizing interfacial DMI and hence, spintronic devices. There is additional interest in developing a greater understanding for DMI materials for applications in spin waves [12], magnetic solitons [13], skyrmions (stable vortexlike magnetic structures) [14], quantum computing [15–19], spintronics [20–23], and other spin-based technologies [24,25].

There have also been a variety of noteworthy nonlinear spin-wave studies with DMI in recent years. The following three examples are representative of the studies. The most recent of the examples, Wang *et al.* studied the magnonic analog to an optical frequency comb (a discrete set of frequencies with equal spacing) [26]. Verba *et al.* did a study of nonlinear spin waves dynamics under the influence of DMI using Hamiltonian formalism [27]. They explored nonlinear spin-wave interactions in a ferromagnetic-heavy-metal bilayer nanowire. Their results offer a means to control signal processing effects in nanowires, as well as using spin-wave amplitude and the nonreciprocal spin-wave dispersion shifts for the possible use in nonreciprocal devices with power dependence. An investigation for the behaviors of spin waves when DMI is present in various ferromagnetic materials was

*jeramy@colorado.edu

performed by Wang *et al.* [28]. Their results may be beneficial for designing magnonic devices such as unidirectional transmission fibers, which use the DMI-induced total reflection of spin waves. Their results offer a means to probe DMI strength as well.

In this paper, we study nonlinear spin waves, and the resulting consequences for FPU, in the presence of DMI. Because the eigenstates are no longer standing waves, we use a discrete Fourier transform analysis method to decompose the signal into its constituent frequencies. The Fourier transform was calculated with a fast Fourier transform (FFT) algorithm as this is more efficient in computational processing. Examining the amplitudes of the FFT gives us a representation of the energy distribution in each mode in the magnetic system. This method can be applied when DMI is present as well as when it is absent. This method also allows us to explore the resulting FPU behavior for a variety of parameters. As such, we investigate the phase diagrams showing how the dynamic magnetic behavior (linear, FPU, or ergodic) depends on the applied magnetic field, the effective anisotropy field, and the initial amplitude for the system with and without DMI.

There are several outcomes of this work that are worth highlighting. First, we study how the onset of the FPU behavior depends on the effective anisotropy field. As a result, we develop an explanation of why uniaxial anisotropy is necessary for the FPU behavior. It turns out the answer is simple. In the one-dimensional chain, solitons only exist in the presence of this anisotropy, and similarly to the elastic system, solitons are a requirement for the FPU behavior. Second, the method developed to characterize eigenstates in the system with DMI works well and reproduces earlier work in standard systems. Finally, in the presence of DMI the initial energy required for the system to transition to the ergodic limit increases substantially. We show that this occurs because the DMI interaction allows a direct nonlinear excitation of more frequencies than are found in a system with only the standard exchange interaction. Thus, the system can accommodate more energy before transitioning to the ergodic limit.

II. BACKGROUND

There are three basic behaviors in the dynamics of nonlinear systems. If we imagine starting the system in an eigenstate or a small combination of eigenstates, then in the linear limit the system remains in the initial state. The second behavior is similar to the classic FPU-like behavior. In this phase the initial state will decompose over time but reconstitute periodically. The third phase is the ergodic phase where the system will have its initial energy thermalize and distribute between all available states, no longer presenting distinguishable wave forms.

Previously, we explored whether FPU-like behavior could be found for a quasi-one-dimensional spin system. We found that some magnetic systems can have FPU-like behavior under specific conditions. Achieving FPU-like behavior expression by the system proved to be anisotropy dependent. Systems with one of the transverse directions being a hard axis and possessing an effective uniaxial anisotropy were successfully tested by starting the system in a low-order magnetic linear eigenstate and varying the amplitude of the initial kick to the system. We characterized the resulting motions by projecting the motion of the magnetization onto a set of linear eigenstates.

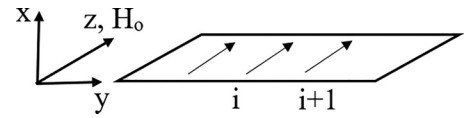

FIG. 1. Schematic illustration of the geometry in this paper. The chain is along the y axis, the applied magnetic field, H_0, is along the z axis, and the spin precession is in the $x-y$ plane. $M(i)$ indexes the site position of the ith spin.

We looked at damping in the system through exploring a dimensionless parameter α. Low damping materials such as Heusler compounds with damping $\alpha \approx 10^{-3}$ [29], cobalt-iron alloys with $\alpha \approx 10^{-4}$ [30], and yttrium iron garnet with $\alpha \approx 10^{-5}$ are available [31,32]. Damping around these values showed clear FPU-like behavior similar to our results without damping.

III. THEORETICAL CONSIDERATIONS

Previously, we explored the FPU-like behavior in our system by looking at the Zeeman, exchange, and anisotropy (or equivalent demagnetization) fields only. We started the quasi-one-dimensional model of N exchange-coupled thin films in a low-order magnetic linear eigenstate. The spin system is illustrated in Fig. 1.

We characterized the resulting motions by projecting the motion of the magnetization onto a set of linear eigenstates, i.e., standing waves, given by Eq. (1). The projection method is normalized by dividing through by the magnetization M.

$$a_n(t) = \frac{1}{N}\left|\sum_{i=1}^{N}\frac{M_y(i,t)}{M}\cos\left[\frac{\pi n(i-1)}{N-1}\right]\right|. \tag{1}$$

When we include the DMI contribution, our equations of motion are given by

$$\frac{d\boldsymbol{M}(i)}{dt} = -|\gamma|\boldsymbol{M}(i)\times\{H_0\hat{z} - 4\pi M_x(i)\hat{x} + J[\boldsymbol{M}(i+1) + \boldsymbol{M}(i-1)] + \boldsymbol{H}_{\rm DMI}(i)\}. \tag{2}$$

$\boldsymbol{M}(i)$ is the magnetization of the ith site of the system along the y direction, the gyromagnetic ratio is given by $|\gamma| = 18.22$ rad/(ns kOe), the applied magnetic field is H_0 applied along $\hat{z}$, the $-4\pi M_x(i)\hat{x}$ provides the effective demagnetizing/anisotropy field for thin films, the magnetization is $|\boldsymbol{M}| = 1.0$ kG, J is the exchange-coupling constant with $JM = 20.0$ kOe, and $\boldsymbol{H}_{\rm DMI}(i)$ is the DMI in the effective field from the DMI as given by Eq. (3).

$$\boldsymbol{H}_{\rm DMI}(i)\begin{cases}\{D_y[M_z(i+1)-M_z(i-1)] - D_z[M_y(i+1)-M_y(i-1)]\}\,\hat{x}\\ \{-D_x[M_z(i+1)-M_z(i-1)] + D_z[M_x(i+1)-M_x(i-1)]\}\,\hat{y}\\ \{D_x\{M_y(i+1)-M_y(i-1)\} - D_y[M_x(i+1)-M_x(i-1)]\}\,\hat{z}\end{cases}. \tag{3}$$

In the one-dimensional chain, with x as the symmetry-breaking direction, only the D_z terms contribute, and the equations of motion become

$$\frac{dM_x(i)}{dt} = -|\gamma|\{J\{M_y(i)[M_z(i+1)+M_z(i-1)] - M_z(i)[M_y(i+1)+M_y(i-1)]\} + M_y(i)H_0 - D_z M_z(i)[M_x(i+1)-M_x(i-1)]\}, \tag{4a}$$

$$\frac{dM_y(i)}{dt} = -|\gamma|\{J\{M_z(i)[M_x(i+1)+M_x(i-1)] - M_x(i)[M_z(i+1)+M_z(i-1)]\} + 4\pi M_x(i)M_z(i) - M_x(i)H_0 - D_z M_z(i) \times [M_y(i+1)-M_y(i-1)]\}, \tag{4b}$$

$$\frac{dM_z(i)}{dt} = -|\gamma|\{J\{M_x(i)[M_y(i+1)+M_y(i-1)] - M_y(i)[M_x(i+1)+M_x(i-1)]\} + 4\pi M_x(i)M_y(i) + D_z\{M_x(i)[M_x(i+1) - M_x(i-1)] + M_y(i)[M_y(i+1)-M_y(i-1)]\}\}. \tag{4c}$$

The total energy of the system is given by Eq. (5) where $\langle i, j\rangle$ refers to summing over nearest neighbors. The first term is the energy from the exchange field, the second term is the DMI contribution, the third term gives the Zeeman contribution, and the fourth term is the effective demagnetization field/anisotropy contribution, where we have added a factor p that allows us to scale this energy.

$$E = -\sum_{\langle i,j\rangle} J(\boldsymbol{M}_i \cdot \boldsymbol{M}_j) - \sum_{\langle i,j\rangle} D_z \cdot (\boldsymbol{M}_i \times \boldsymbol{M}_j) - \sum_i \boldsymbol{M}_i \cdot H_0\hat{z} - \sum_i 2\pi p(\boldsymbol{M}_i\hat{x})^2. \tag{5}$$

As a check, we have insured that energy is conserved for all our numerical results.

IV. IDENTIFYING THE TIME EVOLUTION OF THE NORMAL MODES WHEN DMI IS PRESENT

The spatial projection method used previously no longer works when we include the DMI term because the standing-wave assumption is no longer valid when DMI is included. As mentioned earlier, one has wavelike profiles with a drift velocity but with stationary nodes. These complications bring up the question, how can one decompose the motion of the magnetization into normal modes when DMI is present?

V. TECHNIQUE

We decompose the motion into normal modes by using an iterative overlapping FFT to average the amount of energy in each representative frequency within a given time bin. We refer to this scanning FFT method as binning.

We obtain the M_x, M_y, and M_z time data from the equations of motion, Eqs. (4), by iterating forward numerically using second-order Runge-Kutta integration with a $\Delta t = 10^{-5}$ ns time step. We used typical run times of 130 ns. Run times of 200–350 ns with a time step of $\Delta t = 10^{-6}$ ns were used to check that results were independent of the time step.

We use bins of 16 ns, take an FFT of $M_y(t)$ at each site, find the amplitude for each frequency, and sum the results for each site. Then we plot the summed amplitude for the frequencies to produce a data point for each frequency. The bin is then shifted by 2 ns and the process is repeated. Each FFT gives a snapshot of the energy distribution for central frequency in each bin. When the FFT data points are plotted together sequentially, they trace out the FPU-like frequency modes of the system.

The tunability in the time between the FPU-like recurrences we found in our previous paper was important for our binning method. If the FPU-like behavior peaks are too close together, the FFT has trouble with time resolution. Each bin requires enough total time data to satisfy a small frequency resolution adequate to separate the constituent frequencies. Our frequency resolution is $\Delta f \approx 0.015$ GHz. We tuned the system by using an adequate applied field strength to slow the FPU-like recurrence enough to meet the resolution requirements. We also overlapped the bins to better time-average the data. Figure 2 shows a general example of how the method works. We note that the total energy is conserved despite the changing amplitude in the $M_y(t)$.

The results for the binning method are compared to the results of the projection method in our previous paper in Fig. 3. The DMI field is initially excluded in order to compare the methods. The initial configuration is given by Eq. (6) where A is the initial amplitude, C_1 and C_2 are the percentage for combining the modes, n_1 and n_2 are the respective mode numbers, i is the index for each site, and N is the total number of sites.

$$M_y(i) = A\left\{C_1 \cos\left[\frac{n_1(i-1)\pi}{N-1}\right] + C_2 \cos\left[\frac{n_2(i-1)\pi}{N-1}\right]\right\}. \tag{6}$$

We start the magnetic system in the initial condition with it in $C_1 = 95\%$, $n_1 = 0$ mode and $C_2 = 5\%$, $n_2 = 2$ mode. This initial condition was chosen to introduce asymmetry. We use $N = 256$ spins with an initial amplitude of $A = 0.1$, a time step of $\Delta t = 10^{-5}$ ns, maximum time of $t_{\max} = 200$ ns, and an applied magnetic field of $H_0 = 9.9$ kOe.

The two methods produce very similar results. We evaluate the effective time for an individual bin by simply using the central time of that bin. The amplitudes for Fig. 3(b) have been scaled to match the projection method of Fig. 3(a). As previously stated, the projection method is already normalized.

We now explore the transitions between the linear, FPU-like, and ergodic phases for the cases when DMI is both absent and present. To do this, we use phase diagrams indicating the regions of parameter space where either linear behavior, FPU behavior, or ergodic behavior are found. We use the projection

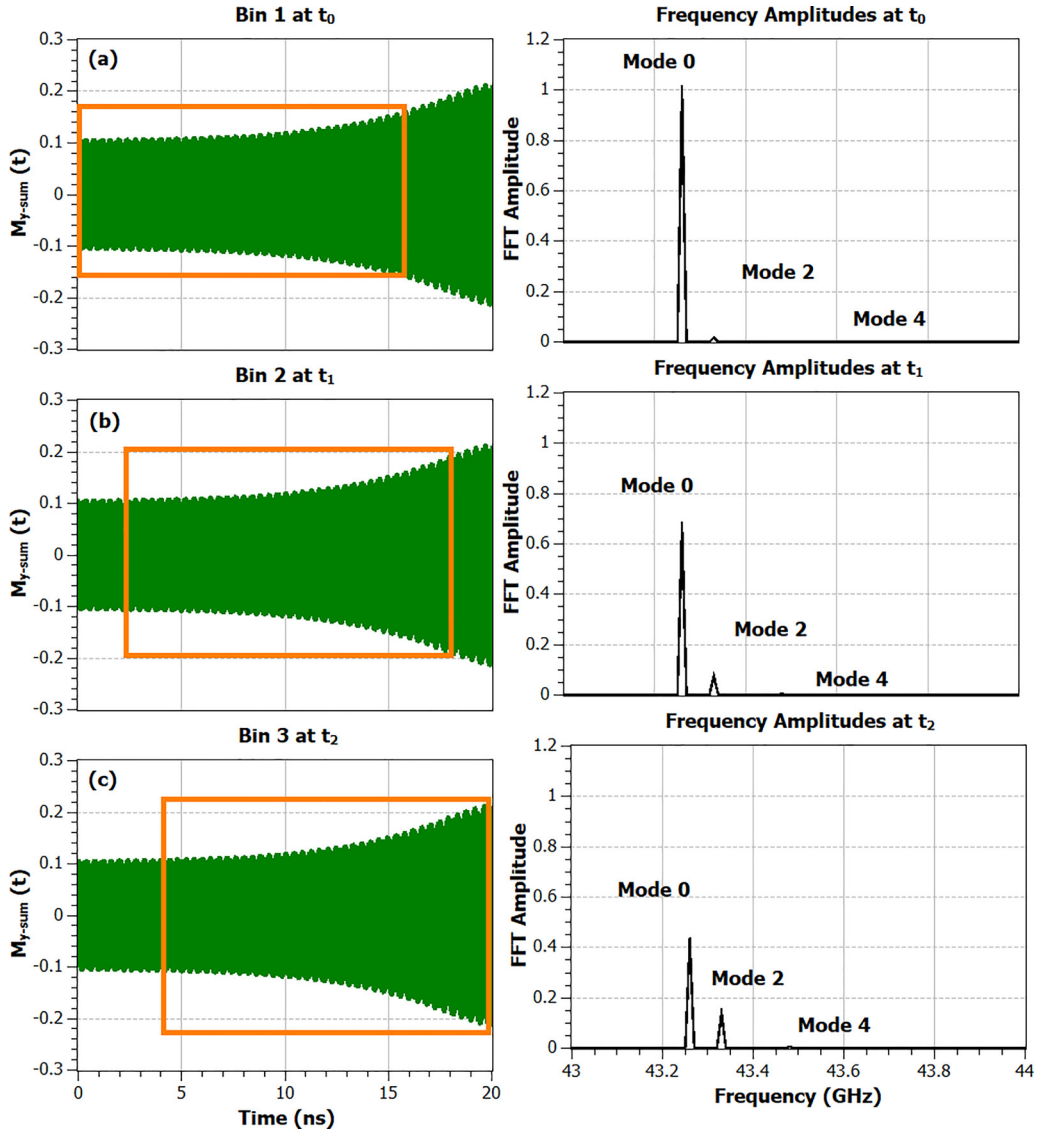

FIG. 2. Illustration of the binning method. We use a bin size of 16 ns indicated by the orange box. As an example, $M_{y-sum}(t) = (1/N)\sum_i M_y(i)/M_s$. We then perform an FFT at each site as described in the text and plot the normalized amplitude of the constituent frequencies. The amplitudes are normalized by dividing by the largest frequency amplitude in the FFT of the data in the first bin, making it 1, to scale all the plots. In (a) the bin starts at $t = 0$. We shift the bin by 2 ns in frame (b) and plot the new FFT data that shows different amplitude strengths. Frame (c) shows the results again with the time bin shifted by an additional 2 ns.

method when DMI is absent and the binning method when DMI is present.

VI. RESULTS

Since the binning method is a different technique, we present Fig. 4 as an example of how the phase regions are classified using the binning method. For this example, the initial state is nearly the same as for Fig. 2 with the exception that the DMI value is set to $D_z M = 2.5$ kOe and the applied field is varied. Since the frequencies no longer show the transition towards ergodic behavior clearly, we change to using the phrase "towards ergodic" to indicate that the number of states is substantially larger, but perhaps not quite the ergodic state yet. The linear, FPU-like, and tending towards ergodic plots are clearly distinct, i.e., in the linear case the amplitudes of the modes are nearly independent of time, as seen in Fig. 4(a). In the FPU domain, the amplitudes of the different modes oscillate in time, as in Fig. 4(b). Finally, in Fig. 4(c) the amplitudes vary irregularly in time. The FFT amplitudes are normalized as discussed earlier. We exclude examples for the projection method since our previous paper shows the plots of the different states.

Figure 5 demonstrates examples of the limiting factors associated with the binning method. The parameters for this figure are $A = 0.5$, $H_0 = 5.0$ kOe and the initial state is started in the $n = 1$ configuration. Figure 5(a) shows the results when the standard projection method is used, and Fig. 5(b) shows the results for the binning method. If the FPU oscillations occur too rapidly, as seen in (a), it will exceed the resolution of the binning method producing vague results as seen in (b).

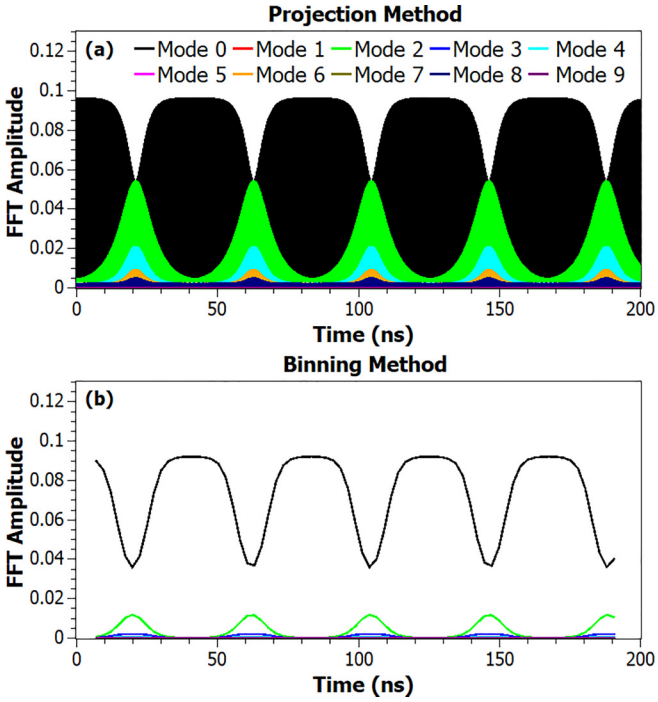

FIG. 3. A comparison of the FPU-like results. The system is started in the 95% $n = 0$ and 5% $n = 2$ states with the initial amplitude $A = 0.1$ for the projection method in (a) and the binning method in (b). The binning method utilizes midpoint values, producing a slight shift in data at the beginning and end of plot (b). In addition, there is a slight distortion of the width of the peaks.

A. Phase diagrams for systems without DMI

We explore how the FPU behavior depends on the parameters of the system through a series of phase diagrams. Initially, in Figs. 6–8, we consider the case where there is no DMI in the system. The system generally uses the same parameters as in Figs. 2–5 but varying the initial amplitude A, applied field strength H_0, and percent strength of the demagnetization field p to create the phase diagram. For each case, the system is started in the $C_1 = 95\%$ for $n_1 = 0$ and $C_2 = 5\%$ for $n_2 = 2$ state. The regions where the system shows linear behavior is below the red boxes; FPU-like behavior is seen in the region between the red and blue boxes, and ergodic behavior occurs above the blue boxes.

Figure 6 explores the phase diagram for the variables applied field and demagnetizing field. The initial amplitude is held constant at $A = 0.12$, so to some extent a larger applied field represents a larger energy for the initial state. We alter the demagnetization/anisotropy field by multiplying it by a value p ranging between 0.0 and 1.5. As the applied field is increased, the phase diagram shows a transition from linear to FPU-like, then to ergodic as expected. As the demagnetization field is reduced, the required applied field amplitude to cause phase transitions increases rapidly, and below about 12% of the demagnetization field, the system remains linear without transitions in the region studied, stressing the importance of the anisotropy provided by the demagnetization field. This is expected as we initially did not see FPU-like behavior [4] until we added the demagnetization field to provide the uniaxial anisotropy. Larger values of the demagnetization field have little effect.

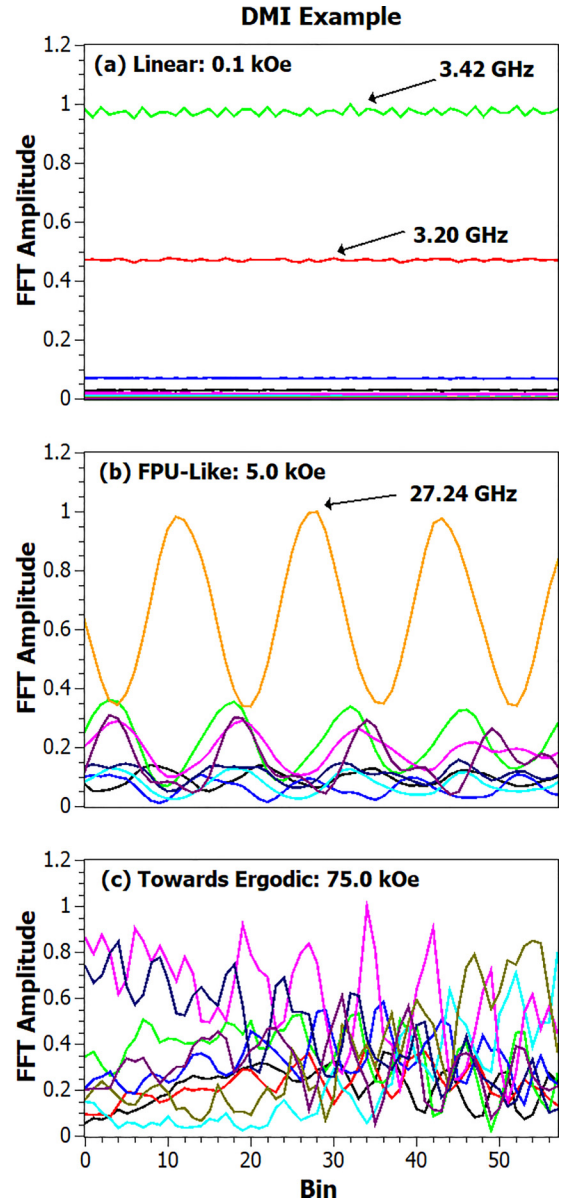

FIG. 4. Examples of linear, FPU, and ergodic behavior for a system with DMI. The system is started the same as in Fig. 2 with the DMI value set to $D_z M = 2.5$ kOe while the applied field is varied. (a) When $H_0 = 0.1$ kOe, the system remains in its initial state with slight oscillations. (b) When $H_0 = 5.0$ kOe the initial state distributes to nearby frequencies but periodically returns to the initial state. (c) When $H_0 = 75.0$ kOe, the characteristic nonlinear behavior of the system evolves towards an ergodic state.

We can understand this behavior in a simple way. As mentioned in the Introduction, the FPU effect is related to soliton motion. As has been shown by Mikeska and others [33,34] in a one-dimensional chain, solitons only exist in the presence of some effective easy-plane anisotropy. For us, this is provided by the effective demagnetizing field. When the demagnetizing field goes to zero, there are no solitons and therefore, no magnetic FPU.

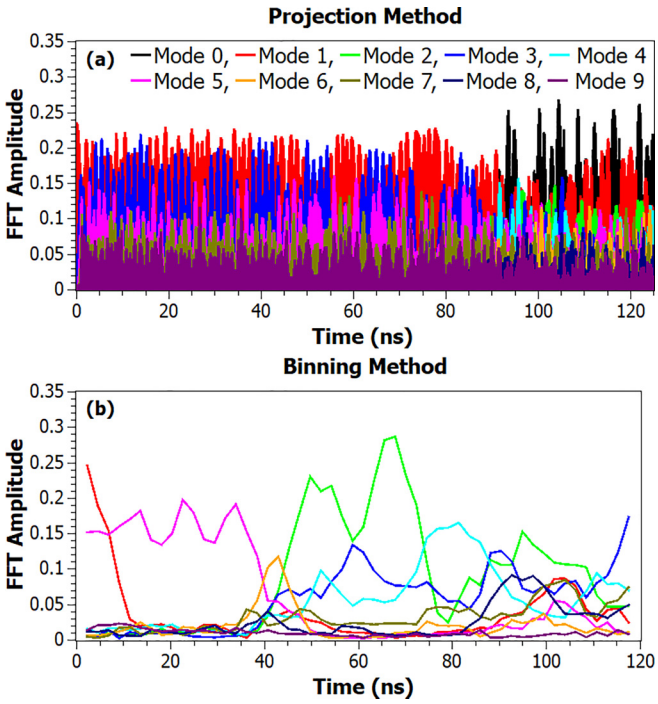

FIG. 5. Example of the ergodic case without DMI. The projection method and the binning method are applied to the same case. The system is started in the $n = 1$ state with $A = 0.5$ and $H_0 = 5.0$ kOe. (a) The projection method shows a clear breaking of the symmetry and ergodic behavior near 90 ns. (b) The frequencies no longer show the transition towards ergodic behavior clearly.

In Fig. 7, we examine the phase diagram for the case where the variables are the initial amplitude and the demagnetization field. The applied field is held constant at $H_0 = 9.9$ kOe. When we increase the initial amplitude of the system, we again increase the energy of the system and the potential for nonlinear behavior. The system requires a larger initial amplitude at smaller demagnetization field strengths to transition from linear to FPU-like and from FPU-like to ergodic behavior. As the demagnetization field is increased to about 50%, the energy appears adequate to allow the ergodic state to be reached at lower initial amplitudes. The FPU-like region has a narrow range of initial amplitudes between the linear and ergodic regions.

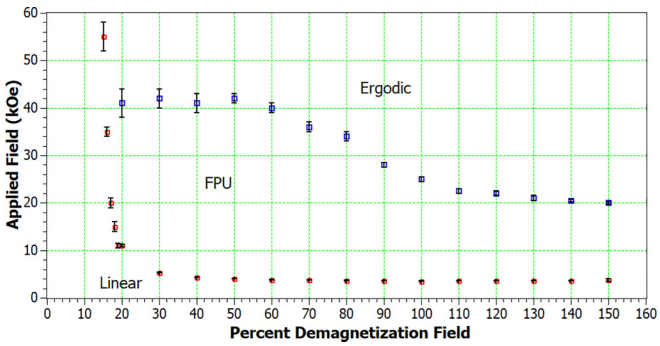

FIG. 6. Phase diagram for the applied field and demagnetization field variables. The system is started in 95% $n = 0$ and 5% $n = 2$ states with the initial amplitude held constant at $A = 0.12$. The FPU state clearly vanishes for low values of the demagnetization field.

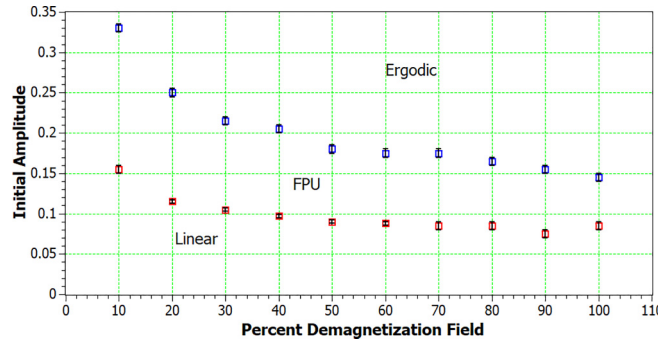

FIG. 7. Phase diagram for the initial amplitude and demagnetization field variables. The system is started in a 95% $n = 0$ and 5% $n = 2$ state with the applied field held constant at $H_0 = 9.9$ kOe. The demagnetization field was incrementally increased from 10% to 100% while varying the initial amplitude to estimate the linear, FPU, and ergodic phase transition conditions.

Figure 8 explores the phase diagram for the variables' initial amplitude and applied field. As the applied field moves from small field to large field, there is an increase in the energy to the system, i.e., the nonlinear terms become more important, and less initial amplitude is required to cause the phase transitions.

B. Phase diagrams with DMI

The introduction of DMI has the potential to make significant changes in the FPU behavior. The reason for this is that, as indicated in the Introduction, the eigenstates of the system are no longer standard standing waves. The nodes remain fixed in time, but the antinodes drift with a constant velocity. We note several recent review articles on DMI and its consequences have recently appeared [35,36].

As before, we investigate the phase transitions for various combinations between the initial amplitude A, applied field strength H_0, and percent strength of the demagnetization field p. Again, the system is started in the 95% $n = 0$ and 5% $n = 2$ state. We now include DMI and hold the DMI constant at

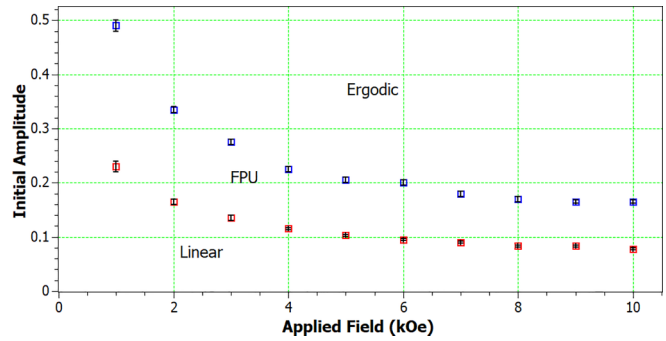

FIG. 8. Phase diagram for the initial amplitude and applied field variables. The system is started in a 95% $n = 0$ and 5% $n = 2$ state with the demagnetization field held constant at 100%. At a fixed field, increasing the amplitude added extra energy to the system, causing transitions from the linear state to the FPU state to the ergodic state.

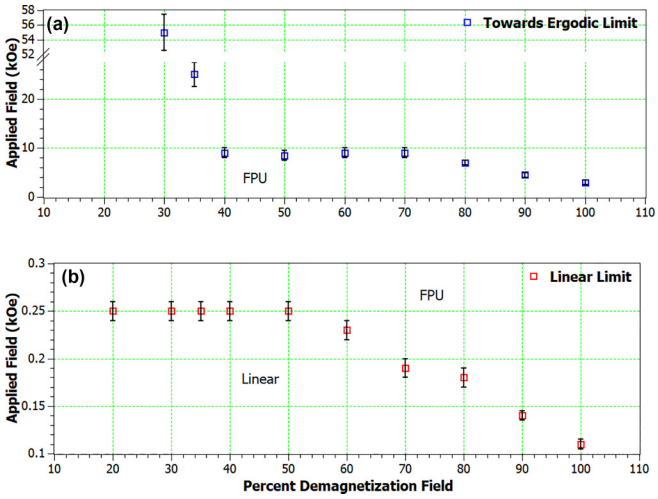

FIG. 9. Phase diagram for the applied field and demagnetization field variables. The system is started in a 95% $n = 0$ and 5% $n = 2$ state with the inclusion of the DMI field set at $D_zM = 2.0$ kOe with the initial amplitude held constant at $A = 0.24$. The FPU-like to ergodic phase transition is seen in (a) while the linear to FPU-like phase transition is seen in (b).

$D_zm = 2.0$ kOe for Figs. 9 and 10. As stated earlier, the boundary between FPU-like and towards ergodic is difficult to distinguish. The criteria we used for determining this region was when the FPU-like behavior was no longer clear and when the FFT amplitude peaks become irregular in time with no distinguishable pattern. Sometimes the FFT amplitude peaks collapse completely, like the example given previously in Fig. 5(b).

When DMI is included, the general shape of the phase diagram in Fig. 9 is similar to that in Fig. 6 where there is no DMI. However, there are some differences. Without DMI the transition from linear to FPU takes place at an external field of about 4 kOe over most of the demagnetization field values. With DMI this same transition now typically occurs near values of 0.25 kOe. In addition, the asymptotic behavior

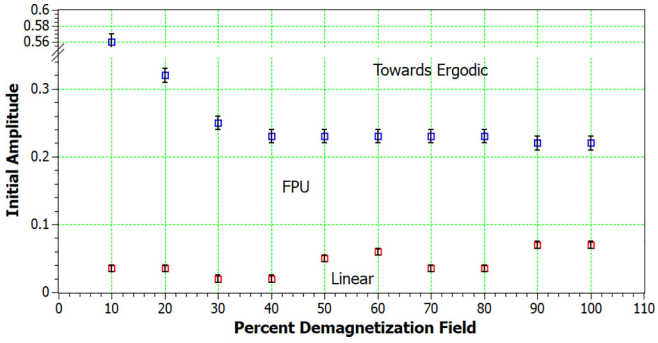

FIG. 10. Phase diagram for the initial amplitude and demagnetization field variables. The system is started in a 95% $n = 0$ and 5% $n = 2$ state with the inclusion of the DMI field set at $D_zM = 2.0$ kOe with the applied field held constant at $H_0 = 6.0$ kOe. The demagnetization field was increased from 10% to 100% while varying the initial amplitude to estimate the linear, FPU, and ergodic phase transition conditions.

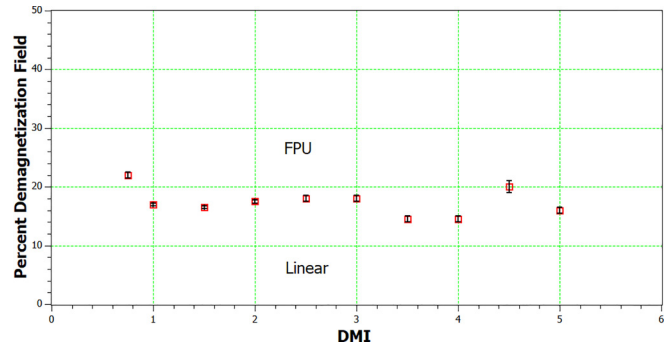

FIG. 11. Phase diagram for the demagnetization field and DMI variables. The system is started in a 95% $n = 0$ and 5% $n = 2$ state with the initial amplitude held constant at $A = 0.12$ with the applied field held constant at $H_0 = 9.9$ kOe. The DMI value is increased from $D_zM = 0.75$ kOe to $D_zM = 5.0$ kOe while varying the demagnetization field strength to estimate the linear, FPU, and ergodic phase transition conditions.

for the FPU/ergodic transition seen at low demagnetization features occurs at a much higher value of the demagnetization field. We suggest that both these features are a result of there being additional nonlinear paths for energy distribution in the system with DMI. This will be explicitly demonstrated later.

In Fig. 10, we create the phase diagram as a function of the demagnetization field strength and the initial amplitude of the system while holding the applied field constant at $H_0 = 6.0$ kOe. In comparison to Fig. 7, the field strength had to be significantly decreased to bring the transition amplitudes down to the same scale as the no DMI case. The requirement for a large decrease in applied field strength again could be a result of there being additional nonlinear paths for energy distribution in the system with DMI.

In Fig. 11, we investigate the phase diagram as a function of the variables, demagnetization field percentage, and DMI strength and hold the initial amplitude at $A = 0.12$ with the applied field at $H_0 = 9.9$ kOe. The first thing to notice is that, for these values, the transition to the ergodic limit occurs at very high demagnetizing fields (or anisotropy values). It is well outside the values in the graph, at times near 5000% of the typical demagnetization field.

We also explored various initial amplitudes ranging between $A = 0.12$ and $A = 0.6$. Increasing the initial amplitude brought the linear to FPU-like transitions to lower and lower anisotropy/demagnetization field strengths. A similar result was previously seen in Fig. 9(b). Pure linear behavior was no longer able to be found after amplitudes reached $A = 0.25$. In all cases, the transition from FPU-like to towards ergodic required excessively large demagnetization fields.

We note that we explored phase diagrams for the initial amplitude/DMI case as well as the applied field/DMI case with unremarkable results.

Figure 12 is a column chart showing how many frequencies engage in the FPU behavior as a function of the DMI coupling constant. We examine three different cases with different applied fields or demagnetization fields while increasing the magnitude of the DMI contribution. The system is started in the 95% $n = 0$ and 5% $n = 2$ state with an amplitude of

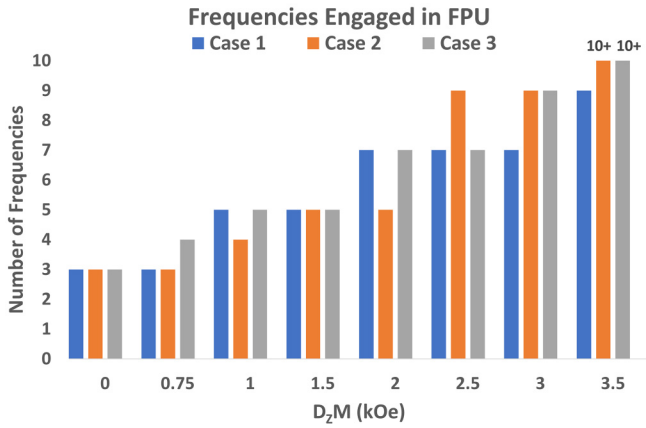

FIG. 12. Column chart depicting the number of frequencies engaged in the FPU behavior. For all three comparisons, the systems are started in a 95% $n = 0$ and 5% $n = 2$ state with an initial amplitude $A = 0.12$. The demagnetization field and applied field were slightly varied for each case. Case 1 has an applied field $H_0 = 9.9$ kOe and the demagnetization field is 100%. Case 2 has an applied field $H_0 = 10.0$ kOe and 100% demagnetization field. Case 3 has an applied field $H_0 = 10.0$ kOe and 95% demagnetization field.

$A = 0.12$ for all three cases. Case 1 has the applied field strength set at $H_0 = 9.9$ kOe and the demagnetization field set at 100%. Case 2 has the applied field set slightly higher at $H_0 = 10.0$ kOe and the demagnetization field set at 100%. Case 3 has the applied field set at $H_0 = 10.0$ kOe and the demagnetization field set at 95%.

We estimated frequency engagement by looking at the FFT amplitudes of the frequencies and whether each frequency possessed oscillatory behavior. To measure engagement, we required that a mode have an amplitude which is 5% or larger compared to that of the mode with the largest amplitude. The increase in the number of frequencies engaged in the FPU behavior as the DMI value is increased suggests and supports that the presence of DMI creates a greater opportunity for the systems energy to distribute through more paths.

VII. CONCLUSIONS

In summary, we address the possibility of FPU behavior in systems both with and without DMI. Because the presence of DMI does not result in standing waves, we introduce a binning method to identify the states present in the system. The binning method is validated by reproducing the known results obtained from the projection method when no DMI is present in the magnetic system. This allows us to explore systems with DMI contributions that otherwise would not have been possible. The method currently has resolution limitations imposed by processor speeds and compromises in data acquisition rates.

The phase diagrams for the magnetic system without DMI contributions confirmed the requirement of having a uniaxial anisotropy present in order to transition from a linear behavior to the FPU behavior. In many systems, a demagnetization field will provide the effective uniaxial anisotropy. Figures 6 and 7 demonstrate that as the initial energy is increased, the system progressively transitions from the linear state to the FPU state and followed by the ergodic state.

When DMI is included in the system, there exists a greater potential for the energy in the system to be distributed to multiple modes. The "towards ergodic" limit can be very large while the linear limit can become very low, as seen in Fig. 10. The existence of a demagnetization/anisotropy field remains critical to the existence of the FPU state. Overall, the FPU-like nonlinear behavior is easier to achieve and more difficult to transition out of when DMI is present.

[1] E. Fermi, J. Pasta, S. Ulam, and M. Tsinguo, Los Alamos Scientific Laboratory Report No. LA1940, 1955 (unpublished) [reprinted in *Nonlinear Wave Motion*, Lectures in Applied Mathematics, edited by A. C. Newell (American Mathematical Society, Providence, 1974), Vol. 15, p. 143].
[2] N. J. Zabusky and M. D. Kruskal, Phys. Rev. Lett. **15**, 240 (1965).
[3] M. Wu and C. E. Patton, Phys. Rev. Lett. **98**, 047202 (2007).
[4] J. Lewis, R. E. Camley, and N. R. Anderson, Phys. Rev. Lett. **120**, 167203 (2018).
[5] D.-H. Kim, S.-C. Yoo, D.-Y. Kim, B.-C. Min, and S.-B. Choe, Sci. Rep. **7**, 45498 (2017).
[6] Z.-D. Li, Q.-L. Bao, P.-B. He, T.-F. Xu, and B. Wu, J. Magn. Magn. Mater. **512**, 166981 (2020).
[7] B. Tang, G.-L. Li, and M. Fu, J. Magn. Magn. Mater. **426**, 429 (2017).
[8] Z.-H. Cheng, W. He, X.-Q. Zhang, D.-L. Sun, H.-F. Du, Q. Wu, J. Ye, Y.-P. Fang, and H.-L. L. Liu, Chin. Phys. B **24**, 077505 (2015).
[9] B. W. Zingsem, M. Farle, R. L. Stamps, and R. E. Camley, Phys. Rev. B **99**, 214429 (2019).
[10] A. Barman, G. Gubbiotti, S. Ladak, A. O. Adeyeye, M. Krawczyk, J. Gräfe, C. Adelmann, S. Cotofana, A. Naeemi, V. I. Vasyuchka *et al.*, J. Phys.: Condens. Matter **33**, 413001 (2021).
[11] J.-H. Moon, S.-M. Seo, K.-J. Lee, K.-W. Kim, J. Ryu, H.-W. Lee, R. D. McMichael, and M. D. Stiles, Phys. Rev. B **88**, 184404 (2013).
[12] J. Mulkers, B. Van Waeyenberge, and M. V. Milošević, Phys. Rev. B **95**, 144401 (2017).
[13] J. Tan, Z.-H. Deng, T. Wu, and B. Tang, J. Magn. Magn. Mater. **475**, 445 (2019).
[14] D. Prychynenko, M. Sitte, K. Litzius, B. Krüger, G. Bourianoff, M. Kläui, J. Sinova, and K. Everschor-Sitte, Phys. Rev. Appl. **9**, 014034 (2018).
[15] V. V. Mazurenko, Y. O. Kvashnin, A. I. Lichtenstein, and M. I. Katsnelson, J. Exp. Theor. Phys. **132**, 506 (2021).
[16] J. Sampaio, A. V. Khvalkovskiy, M. Kuteifan, M. Cubukcu, D. Apalkov, V. Lomakin, V. Cros, and N. Reyren, Appl. Phys. Lett. **108**, 112403 (2015).
[17] L. K. Grover, Phys. Rev. Lett. **79**, 325 (1997).
[18] P. W. Shor, SIAM J. Comput. **41**, 303 (1999).

[19] A. H. Comstock, C-T. Chou, Z. Wang, T. Wang, R. Song, J. Sklenar, A. Amassian, W. Zhang, H. Lu, L. Liu *et al.*, Nat. Commun. **14**, 1834 (2023).
[20] D. Cortés-Ortuño, M. Beg, V. Nehruji, L. Breth, R. Pepper, T. Kluyver, G. Downing, T. Hesjedal, P. Hatton, T. Lancaster *et al.*, New J. Phys **20**, 113015 (2018).
[21] B. H. Zhang, Y. S. Hou, Z. Wang, and R. Q. Wu, Phys Rev. B **103**, 054417 (2021).
[22] Y. Ga, Q. Cui, J. Liang, D. Yu, Y. Zhu, L. Wang, and H. Yang, Phys. Rev. B **106**, 054426 (2022).
[23] J. Liang, M. Chshiev, A. Fert, and H. Yang, Nano Lett. **22**, 10128 (2022).
[24] N. M. Vargas, F. Torres, A. A. Baker, J. R. I. Lee, M. Kiwi, T. M. Willey, C. Monton, and I. K. Schuller, Appl. Phys. Lett. **117**, 213105 (2020).
[25] Z. Wang, Y. Cao, R. Wang, B. Liu, H. Meng, and P. Yan, J. Magn. Magn. Mater. **512**, 167014 (2020).
[26] Z. Wang, H. Y. Yuan, Y. Cao, Z.-X. Li, R. A. Duine, and P. Yan, Phys. Rev. Lett. **127**, 037202 (2021).
[27] R. Verba, V. Tiberkevich, and A. Slavin, Phys. Rev. B **99**, 174431 (2019).
[28] Z. Wang, B. Zhang, Y. Cao, and P. Yan, Phys. Rev. Appl. **10**, 054018 (2018).
[29] C. Sterwerf, S. Paul, B. Khodadadi, M. Meinert, J.-M. Schmalhorst, M. Buchmeier, C. K. A. Mewes, T. Mewes, and G. Reiss, J. Appl. Phys. **120**, 083904 (2016).
[30] M. A. W. Schoen, D. Thonig, M. L. Schneider, T. J. Silva, H. T. Nembach, O. Eriksson, O. Karis, and J. M. Shaw, Nat. Phys. **12**, 839 (2016).
[31] V. Lauer, D. A. Bozhko, T. Brächer, P. Pirro, V. I. Vasyuchka, A. A. Serga, M. B. Jungfleisch, M. Agrawal, Y. V. Kobljansky, G. A. Melkov *et al.*, Appl. Phys. Lett. **108**, 012402 (2016).
[32] H. Chang, P. Li, W. Zhang, T. Liu, A. Hoffman, L. Deng, and M. Wu, IEEE Mag. Lett. **5**, 6700104 (2014).
[33] H. J. Mikeska, J. Phys. C.: Solid State Phys. **11**, L29 (1978).
[34] A. M. Kosevich, B. A. Ivanov, and A. S. Kovalev, Phys. Rep. **194**, 117 (1990).
[35] R. E. Camley and K. L. Livesey, Surf. Sci. Rep. **78**, 100605 (2023).
[36] M. Kuepferling, A. Casiraghi, G. Soares, G. Durin, F. Garcia-Sanchez, L. Chen, C. H. Back, C. H. Marrows, S. Tacchi, and G. Carlotti, Rev. Mod. Phys. **95**, 015003 (2023).